scientific reports

Check for updates

OPEN

STAT1 and m^{6}A-mediated IL15RA upregulation promotes metastasis via ZEB1/NF-κB axis in ccRCC

Jia Wei[1,8], Xuan'er Zhao[2,8], Huiping Wang[3,8], Cong Wang[1], Xinyi Liu[4], Zimeng Shan[5], Yican Guo[6], Xumeng Gu[2], Renren Li[7]✉ & Zhansheng Zhu[1]✉

Interleukin-15 receptor alpha (IL15RA) demonstrates critical regulatory function in oncogenesis and immunomodulation across various malignancies. However, the role of IL15RA in cancers, such as Clear Cell Renal Cell Carcinoma (ccRCC) remains unclear. Therefore, integrated pan-cancer analysis and mechanism investigation assays are essential for IL15RA-directed therapeutic strategy optimization in ccRCC. The comprehensive pan-cancer analysis reveals IL15RA as a plausible diagnostic and prognostic biomarker, as well as a promising immunotherapeutic target across various cancers, particularly ccRCC. IL15RA promotes ccRCC metastasis based on the data of the investigation. Mechanistically, STAT1 binds to IL15RA promoter region, thereby enhancing IL15RA mRNA expression, while METTL3 modulates RNA m^{6}A methylation patterns to stabilize IL15RA transcription. Furthermore, IL15RA potentiates metastasis via NF-κB/ZEB1 axis in ccRCC. Drug sensitivity profiling further indicates that IL15RA expression increases sensitivity to chemotherapeutic agents in ccRCC patients. The findings demonstrate that IL15RA emerges as a critical prognostic indicator and immunotherapeutic biomarker particularly in ccRCC. Our findings underscore the necessity for comprehensive mechanistic studies to elucidate IL15RA's roles and are beneficial for advancing targeted therapeutic strategies in oncological interventions.

Keywords IL15RA, Clear cell renal cell carcinoma, Metastasis, m^{6}A, NF-κB, ZEB1

The global burden of cancer is projected to rise substantially in subsequent decades, attributable to demographic expansion, population aging, and increasing prevalence of established risk factors including tobacco use and adiposity-related pathologies[1]. Contemporary oncological interventions have undergone paradigm evolution, integrating multimodal approaches ranging from surgical excision and cytotoxic chemotherapy to precision radiotherapy and immunomodulatory strategies[2]. Despite these advancements, complete surgical extirpation with histologically negative margins persists as the therapeutic cornerstone for localized solid malignancies[3]. Notably, immunotherapy has emerged as a transformative modality in neoplastic management, demonstrating unprecedented clinical responses across diverse tumor types through strategic modulation of host immune responses.

IL-15 receptor alpha (IL15RA), an emerging therapeutic target in immunotherapy, enhances IL-15 biological activity through formation of a stable IL-15/IL15RA complex that improves cytokine stability and bioavailability[4]. The IL15-IL15RA fusion protein has demonstrated therapeutic efficacy across multiple malignancies, with preclinical evidence supporting its application in melanoma, breast cancer, and colorectal cancer[5,6]. Mechanistically, recent research demonstrates that regular exercise mediates tumor-suppressive effects via IL-15/IL15RA axis activation[7]. Paradoxically, emerging evidence reveals IL15RA + tumor-associated macrophages mediate CD8 + T cell exclusion in breast cancer through IL15Rα-dependent mechanisms within the tumor microenvironment[8]. Significant pathway complexity was highlighted by Wu et al., who identified pancreatic stellate cell-derived IL-15 activates paracrine IL15RA-STAT3-GPX4/

[1]Laboratory of Experimental and Clinical Pathology, Department of Pathology, School of Basic Medical Sciences, Xuzhou Medical University, Xuzhou 221004, China. [2]School of Anesthesiology, Xuzhou Medical University, Xuzhou 221004, China. [3]Department of Genetics, School of Life Science, Xuzhou Medical University, Xuzhou 221004, China. [4]The First School of Clinical Medicine, Xuzhou Medical University, Xuzhou 221004, China. [5]The Second School of Clinical Medicine, Xuzhou Medical University, Xuzhou 221004, China. [6]School of Medical Imaging, Xuzhou Medical University, Xuzhou 221004, China. [7]Center of Healthcare Management, The Affiliated Maternity and Child Health Care Hospital of Xuzhou Medical University, Xuzhou 221009, China. [8]Jia Wei, Xuan'er Zhao and Huiping Wang contributed equally to this work. ✉email: RENRENLI2023@163.com; victorzhu2013@xzhmu.edu.cn

ACSL3 signaling to confer ferroptosis resistance in pancreatic adenocarcinoma[9]. In Clear Cell Renal Cell Carcinoma (ccRCC), IL15RA promotes cancer cell migration and invasion through IL-15 pathway activation[10]. These paradoxical findings underscore context-dependent dual functionality of IL15RA in tumor biology. However, there is still a lack of systematic research on IL15RA in pan-cancer scale. Thus, an integrated systematic pan-cancer scale to evaluate IL15RA's prognostic significance, diagnostic potential, immune modulatory roles, and transcriptional regulation across malignancies, particularly in ccRCC therapeutic development.

The current comprehensive pan-cancer analysis reveals IL15RA as a potential diagnostic and prognostic biomarker, as well as a promising immunotherapeutic target across various cancers, particularly ccRCC. Furthermore, functional assays were conducted validate the findings predicted in the role of IL15RA. Collectively, our research provides novel insight for IL15RA in precision medicine and therapeutic implications for immunotherapy optimization.

Materials and methods

Dataset collection

Phenotype data of pan-cancer in The Cancer Genome Atlas (TCGA) and normal tissues in Genotype-Tissue Expression (GTEx) database was downloaded from the UCSC Xena Browser (https://xenabrowser.net/). Our team extracted the expression data from GTEx database (https://www.gtexportal.org/) and TCGA database (https://portal.gdc.cancer.gov/). Shiny app names TFTF united Four web tools, namely hTFTarget (http://bioinfo.life.hust.edu.cn/hTFtarget/), ENCODE(http://amp.pharm.mssm.edu/Harmonizome/dataset/ENCODE+Transcription+Factor+Targets), KnockTF (http://www.licpathway.net/KnockTF/), and CHIP_Atlas (https://chip-atlas.org/) were used to analyze the upstream transcription factor regulating IL15RA[11]. Many cancer-related datasets were obtained from the Gene Expression Omnibus (GEO, https://www.ncbi.nlm.nih.gov/geo/) database, namely GSE16441, GSE16449, GSE36895, GSE66270, GSE66271, GSE66272, GSE71963 and GSE76351. The log2 (TPM + 1) transformed normalized expression profiles of the data referred.

Expression and prognosis analysis

HPA database (https://www.proteinatlas.org/) was used to analyze the protein and mRNA expression of IL15RA in multiple tissues. TIMER2.0 database was applied to analyze the differential expression of IL15RA between normal and tumor tissues in cancers across TCGA[12]. Paired differential analysis of IL15RA expression was performed by the R package 'TCGAplot' (Version 7.0.1)[13]. The prognosis data from the UCSC Xena database was downloaded to analyze the expression of IL15RA between OS, DSS, DFS, PFS across cancers of TCGA with Univariate Cox analysis according to the previous study[14]. KMplot analysis was performed on GEPIA2 or UALCAN database, survival that with p value < 0.05 was selected[15,16]. Pan-cancer diagnostic analysis was performed by the function of ROC in 'TCGAplot'.

Expression quantitative trait locus analysis on IL15RA

eQTL (expression quantitative trait locus) and pQTL (protein quantitative trait locus) analysis was performed by DMRdb database (http://www.inbirg.com/DMRdb/#/base)[17]. To further analyze IL15RA by Mendelian randomization (MR) analysis, Two-sample MR analyses were applied to infer causal relationships between modifiable exposures and disease outcomes through the 'TwoSampleMR' R package (version 0.6.3) under the standard: identify strongly associated Single nucleotide polymorphisms (SNPs) ($p < 5e\text{-}08$) as instrumental variables. Linkage disequilibrium parameters were set at $r^2 < 0.001$ and clumping distance = 10, 000 kb. SNPs with weak associations or insufficient explanation of phenotypic variance were excluded, applying a filter of "F-test value > 10". Exposure and outcome were obtained from online IEU OpenGWAS project website (https://gwas.mrcieu.ac.uk/). The IL15RA eQTL genetic data consisted of 31,684 samples and 22,685 SNPs. During the analysis, the inverse variance weighted (IVW) approach was deemed the main outcome of this study, compared with the others (the MR Egger method, the weighted median method, the weighted mode method, and the simple mode method). p values below 0.05 were set as cut-off values and deemed to be statistically significant. In addition, we also applied sensitivity analyses in this study, such as heterogeneity, pleiotropy, and leave-one-out analysis, to assess the stability of our outcomes. Sensitivity analyses ensured the MR exclusivity assumption.

Clinical relationship analysis of IL15RA

The relationship between IL15RA expression with clinical features based on the TCGA data was analyzed on the Sangerbox platform[18]. Detailed demographic information of the TCGA data was directly downloaded from the UCSC Xena Browser and the parameters including clinical Grade, Stage and TNM stage. The differences were shown in cancers that with available data. The correlation results between IL15RA expression at pan-cancer level and clinical Grade, Stage and TNM stage were downloaded for further analysis.

Gene set enrichment analysis (GSEA) of IL15RA

To assess the biological function of IL15RA in tumors, the expression of IL15RA and other genes expression data was retrieved from TCGA database to perform association analysis by batch Pearson's correlation analysis methods. According to the level of the correlation index between other genes and IL15RA, the most associated genes with IL15RA expression were selected to perform the enrichment analysis. GSEA analysis based on predefined gene sets from the Molecular Signatures Database v5.0 was conducted using

the R package 'clusterProfiler' (version 4.6.2)[19]. In the present study, the 'c2.cp.kegg.v7.5.1.entrez.gmt' and 'c5.go.bp.v7.5.1.entrez.gmt' collection sets were used for GSEA[20].

Immune related analysis of IL15RA

Transcriptome data and clinical data were downloaded from the TCGA database for immune related analysis. Immune related analysis of IL15RA was performed on 'TCGAplot' that has been referred before. Correlation analysis was performed between IL15RA expression and immune scores, immune suppressive molecules, immune stimulatory molecules, immune checkpoints, immune cells and immune chemokines as previously reported[21]. These immunomodulators were collected from Charoentong's study[22]. TIDE (http://tide.dfci.harvard.edu/) was used to validate the prediction performance of IL15RA expression in human ICB therapy cohorts by applying the receiver operating characteristic (ROC) which measures the true-positive rates against the false-positive rates, and the area under the ROC curve (AUC) is an effective measure of accuracy. An AUC value of 0.5 represents the performance of the random predictor[23,24]. Immunotherapy response both in vivo and in vitro was predicted by TISMO database (http://tismo.cistrome.org/)[25]. TCIA database (https://tcia.at/home) was used to explore the relationship between IL15RA expression and immune phenotype scores (IPS) in the context of genotype-immunophenotype relationships and prediction of ICB therapy response[22].

Mutation and epigenetic modification analysis of IL15RA

To clarify the genetic mutation features of IL15RA, the 'Cancer Types Summary' module was applied in cBioPortal web (https://www.cbioportal.org/). The correlation between IL15RA levels and other genetic mutation status in these cancers was analyzed by the muTarget dataset (https://www.mutarget.com/analysis?type=target)[26]. The correlation between IL15RA and TMB or MSI was assessed using Pearson correlation analysis, and the radar plot was drawn with the 'fmsb' R package (version 0.7.5) based on 'TCGAplot' that have been referred before. GSCA database (https://guolab.wchscu.cn/GSCA/#/) was applied to estimate the correlation between IL15RA expression and methylation, copy number variation (CNV). The expression correlation between IL15RA and DNA methyltransferase genes, mismatch repair genes, m^1A, m^6A, and m^5C genes was downloaded and analyzed with R package 'corrplot' (version 0.92).

Single-cell expression analysis of IL15RA

Single-cell expression analysis of IL15RA was performed with Tumor Immune Single-cell Hub (TISCH2) database (http://tisch.comp-genomics.org/)[27,28]. R package 'Seurat' was used to perform the single-cell analysis. The expression data of IL15RA mRNA in different cell types of 9 datasets was downloaded and presented graphically using the R package 'pHeatmap' (version 1.0.12). In addition, UMAP plots showing the expression pattens of IL15RA in different cell types were obtained from the TISCH2 database. GSE159115 data was downloaded from TISCH2 database to perform further analysis by using R package 'Seurat' (version 4.4.0) and 'Scillus' (version 0.5.0).

Cell culture and plasmids

Human RCC cell lines (786-O, 769-P, ACHN, OSRC-2 and Caki-1) and a human renal proximal tubular epithelial cell line (HK2) were purchased from the Chinese Academy of Sciences. 786-O, 769-P and ACHN were cultured in RPMI 1640 (Gibco, USA) supplemented with 10% FBS. OSRC-2, Caki-1 and HK2 were cultured in DMEM supplemented with 10% FBS. The incubation environment was at 37 °C with 5% CO_2.

The full-length cDNA sequence of METTL3, IL15RA or STAT1 was directly synthesized by Genewiz Company (China) and cloned into the plasmid pcDNA3.1(+) (Invitrogen, USA) for gene overexpression. The above plasmids were transfected into cells cultured for 48 h in a 6-well plate. For IL15RA silencing, cells were transfected with IL15RA Human shRNA Plasmid Kit (Locus ID 3601, OriGene, USA).

RNA extraction and qRT-PCR

Extraction of total RNA and procedures of qRT-PCR were performed as previously described[29]. The primers for IL15RA, METTL3, STAT1 and GAPDH were listed in Table S1.

Western blotting

Cells were lysed in 1× SDS sample buffer and the concentration of protein sample was measured by the BCA method (Beyotime, China). Then, 20 μg samples were separated using 10% SDS/PAGE and transferred to nitrocellulose membranes. After blocking in 5% skim milk at room temperature for 1 h, the membranes were probed with primary antibodies against IL15RA, METTL3, p-p65, STAT3, β-Actin and GAPDH (Abcam, USA).

Dual luciferase assay

The full 500 bp promoter sequence from upstream of Transcription start site of human IL15RA and the −456 bp to −448 sequence deleted mutated promoter sequence were sent to direct synthesis (Sangon, China), then the products were subcloned into the pGL3 Basic luciferase report vector (Promega, USA) at the *Bgl*II and *Hind*III restriction enzyme cutting sites respectively and finally labeled pGL3-full and pGL3-mutated. ACHN cells were seeded 2.5×10^6 cells per well in 6-well plates (Corning, USA). After 16 h, cells were separately transfected with the two constructs (pGL3-full and pGL3-mutated) and empty vector by Lipofectamine 3000 (Thermofisher, USA). 500 ng pGL3-full or pGL3-mutated and 50 ng pRL-TK vector (Promega, USA) were co-transfected for each well. The empty pGL3 Basic vector was taking

as negative control. 24 h after transient transfection, cells were collected for the dual Luciferase reporter assays according to the protocol from Dual-Luciferase® Reporter Assay System kit (Promega, USA).

The m^{6}A modification sites for IL15RA were predicted by the online tool SRAMP[30]. For m^{6}A modification site determination, an METTL3 overexpression plasmid together with wild-type (IL15RA-Luc-WT) or mutated IL15RA plasmids (IL15RA-Luc-MUT1, IL15RA-Luc-MUT2, IL15RA-Luc-MUT3 and IL15RA-Luc-MUT4), were transfected into ACHN or OSRC-2 cells by using Lipofectamine 3000. After 36 h transfection, the cells were lysed by passive lysis buffer. Firefly and Renilla luciferase activity were measured by the Dual-Luciferase Reporter Assay System (Promega, USA).

The p-p65 binding sites for human ZEB1 were predicted by the Eukaryotic Promoter Database EPD[31]. For p-p65 binding sites determination, an IL15RA overexpression plasmid together with PGL3-Basic or ZEB1 plasmids (PGL3-ZEB1-FL, PGL3-ZEB1-MUT1, PGL3-ZEB1-MUT2 and PGL3-ZEB1-MUT3), were transfected into HEK 293 T cells by using Lipofectamine 3000. The following procedures are similar to that for m^{6}A modification site determination.

MeRIP-PCR

The RIP assay was carried out with an EZ-Magna RIP Kit (Millipore, USA), according to the manufacturer's instructions. Briefly, the whole-cell lysate was incubated with RIP buffer containing magnetic beads containing m^{6}A antibody (Epigentek, USA) at 4 °C for 6 h. Finally, the coprecipitated RNAs were analyzed by qRT-PCR.

RNA decay assay

HEK 293 T cells were seeded in 6-well plates overnight, and the METTL3 expression plasmid was transfected into the cells for 24 h. Then ActD (MedChemExpress, USA) was added to inhibit gene transcription for different time spots as indicated. The total RNA was subsequently extracted and analyzed by qRT-PCR. The mRNA half-life ($t_{1/2}$) of IL15RA was calculated using $\ln^{2/slope}$.

Wound healing and transwell migration test

ACHN or OSRC-2 cells were seeded into 6-well culture plate and was gently scratched with a new 200 µL pipette tip across the center of the attached cells (0 h). Cell migration was photographed using microscopy (Leica, Germany) and a 10× objective at the 12 h after injury.

The migratory capacities of cells were evaluated via the transwell assay. All cells were counted in five randomly chosen microscopic fields.

Nude mice tests

BALB/c nude mice (5 weeks old male), purchased from Beijing Vital River Laboratory Animal Technology Co., Ltd. (China), were randomly divided into 3 groups (4 for each group in proliferation, 5 for each group in metastasis) for nude mice assays. For cell proliferation in vivo, stable transfection of OSRC-2 Cells with vector-IL15RA or shIL15RNA was performed. Cells (7×10^6) transfected with vector-IL15RA or shIL15RNA were inoculated subcutaneously into the left side of each mouse body. Tumor size was measured weekly. For cell metastasis in vivo, 3×10^5 cells with vector-IL15RA or shIL15RNA were injected intravenously via the tail vein into each mouse in a laminar flow cabinet. 5 weeks after injection for cell proliferation model, and 7 weeks after injection for tumor metastasis model, mice were then sacrificed with carbon dioxide euthanasia and examined. Final tumor weights were measured.

Ethical statement

The study has been reported in line with the ARRIVE guidelines 2.0. The procedures were examined and verified by Laboratory Animal Ethics Committee of Xuzhou Medical University in accordance with Guide to Laboratory Animal Ethics Examination of Xuzhou Medical University. The relative animal experiments are permitted. The animal test was approved by the Institutional Animal Care and Use Committee at Xuzhou Medical University (No.202207S064).

Drug sensitivity analysis

The Genomics of Drug Sensitivity in Cancer (GDSC) database as benchmark dataset which is downloaded from website (http://www.cancerrxgene.org/) by Wellcome Trust Sanger Institute. The dataset consists of 1001 cancer cell line and 265 tested drugs. Data of the GDSC database was used to analyze the drug sensitivity between the IL15RA-high and IL15RA-low group in TCGA-KIRC[32]. The analysis was performed by R package 'oncoPredict' (version 1.2)[33]. p value < 0.05 was regarded as specific drug sensitive.

Statistical analysis

All statistical analyses were conducted using GraphPad Prism version 10.0 (GraphPad Software, USA). The parametric test (student's *t* test) or nonparametric test (Wilcoxon rank-sum test) was used for comparisons between two experimental groups. Pearson coefficients were calculated to assess potential correlations. All quantitative experimental data was from at least three repeated experiments and was presented as mean ± SD. p value < 0.05 was considered statistically significant ($^*P < 0.05$; $^{**}P < 0.01$; $^{***}P < 0.001$).

Results

IL15RA acts as a promising clinical biomarker for cancers

Expression analysis from the Human Protein Atlas (HPA) database revealed that the IL15RA protein is widely expressed in human tissues (Figure S1A). The similar trend was found in IL15RA in tissues based on

GTEx and HPA data (Figure S1B-C). Furthermore, IL15RA expression exhibits strong positive correlation with IL15, IL2, IL2RA, IL2RB, IL2RG at pan-cancer level (Fig. 1A).

Next, based on DMRdb database, systemic eQTL and pQTL analysis of IL15RA was performed to find that IL15RA may correlate with several diseases including neoplasms. Detailed data was shown in Table S2-S3. Therefore, the subsequent research was mainly on the correlation of IL15RA and neoplasms. The results that comply with the standard of p value < 0.05 was chosen and displayed in Table S4-S5.

In pan-cancer scale, IL15RA was upregulated in various cancers including KIRC (ccRCC), and downregulated in some other malignancies (Figure S1D and Fig. 1B). Further survival analysis demonstrated that high IL15RA expression is associated with poor prognosis in a variety of cancers, especially in KIRC (ccRCC). However, the favoured DSS was found only in PRAD (Fig. 1C).

The above data implied that IL15RA may be a promising prognosis and diagnosis biomarker for various cancers. Pan-cancer OS and RFS Survival Map analysis of IL15RA was conducted to confirm that IL15RA is a potential prognosis indicator for multiple cancers (Fig. 1D-F). Additionally, it was found that IL15RA shows higher diagnosis capability in various cancers including ccRCC (Fig. 1G). The results revealed that IL15RA expression is abnormal in various tumors and performed as a plausible diagnosis and prognosis biomarker of multiple tumors especially in ccRCC.

The association between IL15RA and clinical parameters such as stages, grade, pathological TNM stage was then analysed, the data showed that higher IL15RA level is related to advanced stage, higher grade, and higher TNM stage in multiple cancers, especially in ccRCC (Fig. 1H-L).

IL15RA is associated with cancer-related pathways, biological processes and cancer immunity potency

As shown in Fig. 2A-B, several cancer-related pathways are significantly enriched, biological processes such as wound healing, epithelial to mesenchymal transition, oxidative phosphorylation were highlighted. Notably, lymphocyte activation regulation and immunity response were enriched across all malignancies (Fig. 2B). Further analysis based on CancerSEA database demonstrated that IL15RA exhibits strong correlation with Metastasis, Invasion, Inflammation, Differentiation, and Angiogenesis in multiple cancers including ccRCC (Fig. 2C).

Based on the strong immunity link, immunotherapy potency analysis was performed to evaluate the potential of IL15RA. As Fig. 2D indicated, a positive link between IL15RA expression and immune scores was found in most cancers. Meanwhile, IL15RA exhibited strong correlation between immune suppressive molecules, immune stimulatory molecules (Fig. 2E-F). More interestingly, IL15RA expression displayed a strong relationship with genes associated with immune checkpoints and immune chemokines (Fig. 2G-H). Immune cell analysis revealed that IL15RA is positively correlated with several types of cells such as CD8 + T cells, M1 macrophages, activated NK cells. At the same time, IL15RA expression exhibits negative correlation with cells such as M2 macrophages, memory B cells (Fig. 2I). These results together inferred that IL15RA has high potency in cancer immunotherapy.

Immunotherapy prediction, mutation and other modification analysis of IL15RA

A comparative analysis of the biomarker value of IL15RA and other published biomarkers was further conducted to assess their predictive power for response outcome. Among the 25 examined studies, IL15RA exhibits AUC values greater than 0.5 in 17 studies, suggesting that it may serve as an excellent predictive biomarker (Fig. 3A). IL15RA demonstrated high predictive capabilities for the effects of immunotherapy in 13 cohorts in an in vivo tumor model, as well as for the response to cytokine treatments in 10 cohorts using in vitro cell lines (Fig. 3B-C). Moreover, further analysis showed a positive correlation between IL15RA expression and ips_CTLA4_pos_PD1_pos, ips_CTLA4_neg_PD1_pos in most cancers including ccRCC (Fig. 3D). These results revealed that high expression of IL15RA may better predict the efficiency of immune therapy, especially the efficiency of anti-PD1 therapy.

The potential regulation network of IL15RA expression is the necessary concern of our druggable target. The gene mutation was firstly analyzed. IL15RA exhibited lower mutation frequency in various cancers including ccRCC (Fig. 3E). By using muTarget database, it was found that mutations of other genes may have influence on IL15RA expression in various cancers such as TP53 mutation, which may result in IL15RA expression elevation in cancer (Figure S2A-AJ). Further DNA methylation status analysis showed that DNA methylation exhibits negative correlation with IL15RA expression (Fig. 3F). The link of IL15RA and associated DNMT genes was also analyzed. It is obvious that DNMT1 was strongly correlated with ccRCC (Fig. 3G). Moreover, CNV was considered to have positive relationship with IL15RA expression (Fig. 3H). Additionally, MSH6 exhibited strong correlation with IL15RA in ccRCC (Fig. 3I). RNA methylation was related with ccRCC, especially in m^6A manner (Fig. 3J-L). Transcription activity of IL15 expression was predicted to be modulated by many transcription factors including STAT1 (Figure S3A-B). The correlation between IL15RA expression and TMB and MSI was evaluated to find that only TMB of ccRCC linked to IL15RA (Figure S3C-D). Obviously, kidney cancer shows strong link with IL15RA in gene regulation levels.

Expression, prognosis and single-cell analysis of IL15RA in CcRCC

The role of IL15RA was further explored in kidney cancer. IL15RA is down-regulated in KICH and KIRP, but up-regulated in KIRC (Fig. 4A). The median based KMplot analysis of IL15RA showed statistical differences, a trend of unfavorable prognosis can be observed (Fig. 4B-C). However, the prognosis of IL15RA in KICH showed no significance (data not shown). Data from GEO datasets showed that IL15RA expression was up regulated in ccRCC tissues (Fig. 4D). This result confirmed our previous presumption that IL15RA is a potential diagnostic biomarker.

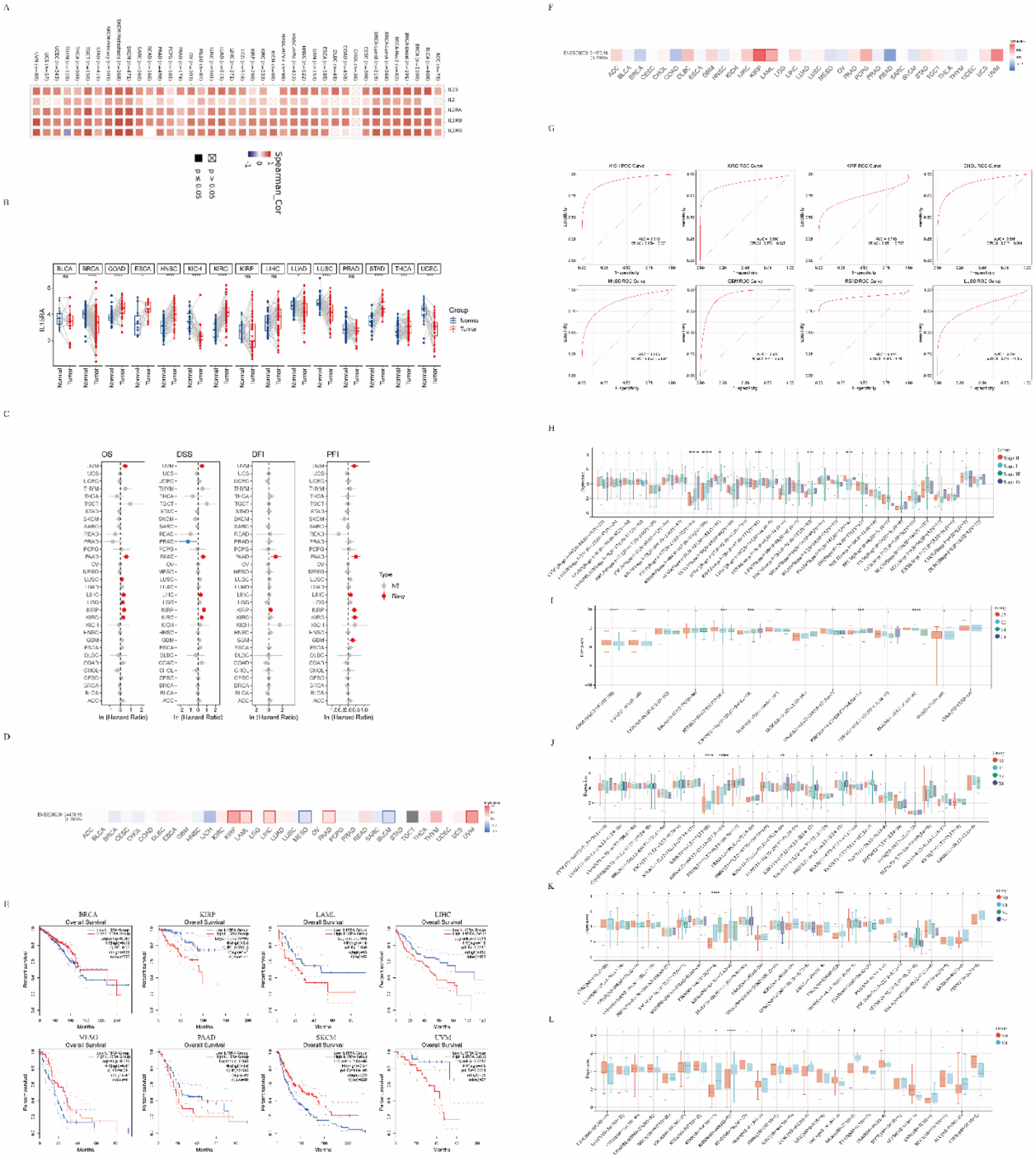

Fig. 1. IL15RA acts as a promising clinical biomarker for cancers. (A). The correlation between IL15RA expression and IL15, IL2, IL2RA, IL2RG. (B). Paired expression of IL15RA in 33 types of tumors. (C). Univariate Cox analysis of IL15RA and OS, DSS, DFI, PFI at pan-cancer level. (D). Kaplan-Meier analysis of the relationship between IL15RA expression and survival features of tumors in TCGA database, OS Survival Map. (E). OS KMplot analysis of BRCA, KIRP, LAML, LIHC, MESO, PAAD, SKCM, UVM. (F). RFS Survival Map. (G). Diagnosis analysis of IL15RA.ROC analysis of the relationship between IL15RA and clinical diagnosis of tumors in TCGA. IL15RA can better predict cancer diagnosis in KICH, KIRC, CHOL, HNSC, GBM, READ, STAD, and UCEC. (H). Analysis of the expression difference of the IL15RA gene in samples of different clinical stages in each tumor. (I). Analysis of the expression difference of the IL15RA gene in samples of different clinical grades in each tumor. (J). Analysis of the expression difference of the IL15RA gene in samples of different clinical T stages in each tumor. (K). Analysis of the expression difference of the IL15RA gene in samples of different clinical N stages in each tumor. (L). Analysis of the expression difference of the IL15RA gene in samples of different clinical M stages in each tumor. $^{*}P<0.05$; $^{**}P<0.01$; $^{***}P<0.001$; $^{****}P<0.0001$.

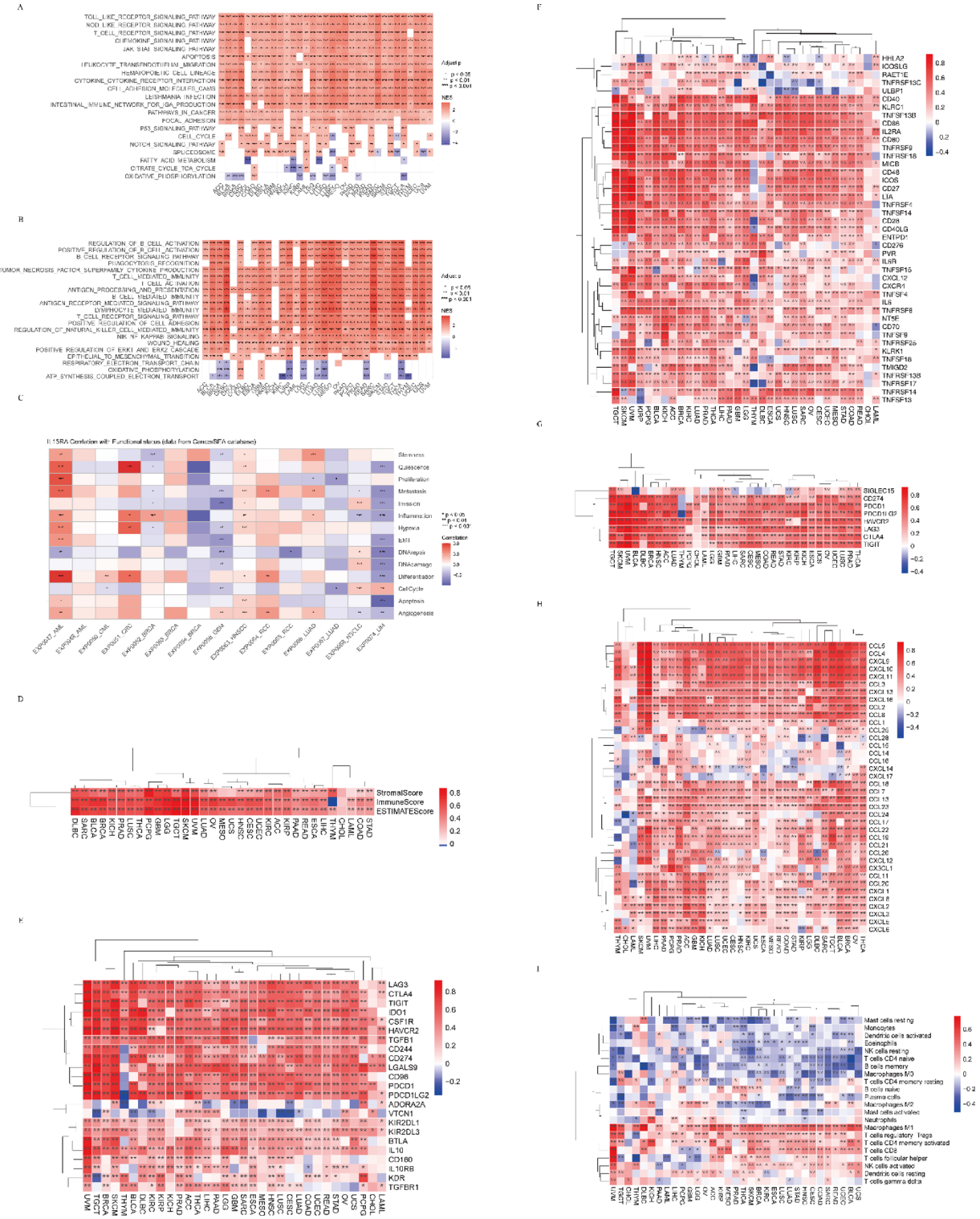

Fig. 2. IL15RA is associated with cancer-related pathways, biological processes and immunity potency. (A). Heatmap showing the Kyoto Encyclopedia of Genes and Genomes pathways related to IL15RA based on GSEA Color ranging from blue to red represents the NES value. (B). Heatmap showing the biological processes related to IL15RA based on GSEA. Color ranging from blue to red represents the NES value. (C). Heatmap showing the correlation between IL15RA expression and 14 kinds of phenotypes based on the CancerSEA database. (D). Immune-related analysis of IL15RA at pan-cancer level. IL15RA expression with immunescore. (E). IL15RA expression with immuinhibitor. (F). IL15RA expression with immustimulator. (G). IL15RA expression with checkpoint. (H). IL15RA expression with chemokine. (I). IL15RA expression with immune-cells. $*P<0.05$; $**P<0.01$; $***P<0.001$; $****P<0.0001$.

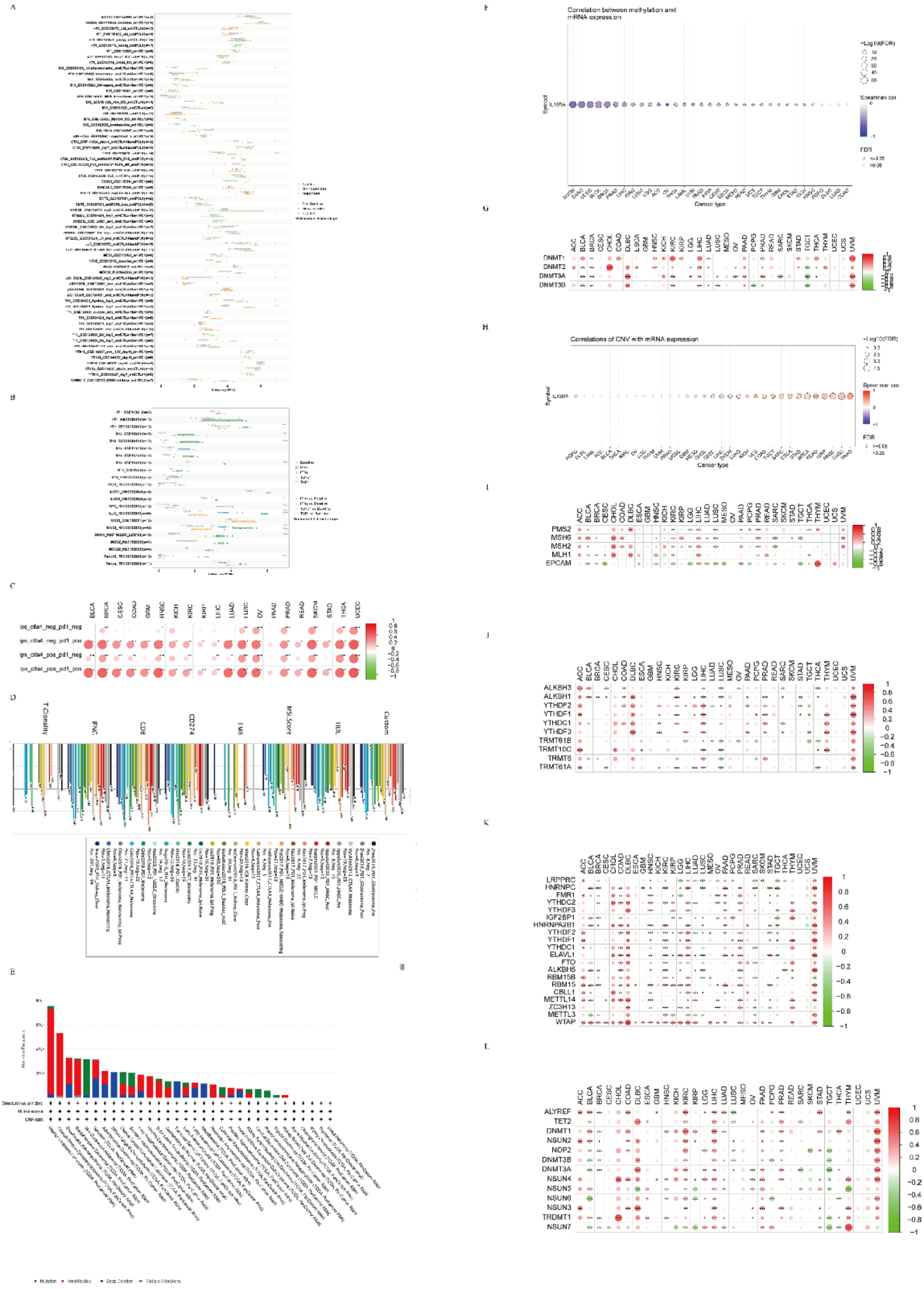

As shown in Fig. 4E, the heatmap, illustrating the relative expression levels of IL15RA across 16 cell types, indicated widespread expression of IL15RA in various immune, stromal and malignant cells. For instance, UMAP plots revealed the expression of IL15RA in CD8 + T cell, Epithelial cell, Malignant cell, Endothelial cell, Monocyte and Macrophage in KIRC (Fig. 4F-G). By analyzing the single-cell dataset GSE159115, the differences were found in the expression of IL15RA between epithelial cells, endothelial cells, malignant cells, and monocytes/macrophages in tumors and normal tissues (Fig. 4H). Besides, IL15RA expression was defined as positive and negative cells based on its expression in various cell types (Fig. 4I). Therefore, differential analysis was conducted between IL15RA positive and negative cells in endothelial cells,

◀**Fig. 3**. Immunotherapy prediction, mutation and other modification analysis of IL15RA. (A). Immunotherapy response of IL15RA in vivo tumor model in murine ICB therapy cohorts. (B). Immunotherapy response of IL15RA in vitro cell lines. (C). The association between IL15RA and IPS scores using the TCIA database. (D). Biomarker relevance of IL15RA compared to standardized biomarkers on tumor immune evasion in ICB therapy cohorts. (E). Mutation and other modification analysis of IL15RA.Genetic alteration frequency of IL15RA. (F). Correlation between methylation and IL15RA expression. (G). Expression correlation of DNA methyltransferase genes with IL15RA. (H). Correlation of CNV with IL15RA expression. (I). Correlation between mismatch repair genes and IL15RA expression. (J). Correlation analysis of IL15RA and m1A genes. (K). Correlation analysis of IL15RA and m6A genes. (L). Correlation analysis of IL15RA and m5C genes. $^{*}P<0.05$; $^{**}P<0.01$; $^{***}P<0.001$.

epithelial cells, malignant cells, and mono/macrophage, and GSEA enrichment analysis was performed (Fig. 4J). The oxidative phosphorylation pathway, hypoxia, inflammation, and EMT pathway in the results had good qualitative consistency with the data from pan-cancer analysis.

STAT1 and m^{6}A-mediated IL15RA upregulation enhances cell migration of CcRCC

Based on the bioinformatic analysis, the role of IL15RA and its modulators in ccRCC is worthy to explore with experiments. The protein expression of IL15RA was detected in five ccRCC cell lines and HK-2 cell line. Apparently, IL15RA showed increased expression in OSRC-2 and ACHN cell lines (Fig. 5A-B). As Fig. 5C showed, with STAT1 overexpression (Figure S4A) in ACHN cell line, The plasmid with binding region has much higher luciferase activity than that with binding region mutated ($P<0.001$). Given the indication from Fig. 3 K, m^{6}A modification mediated by METTL3 is hypothesized to function in IL15RA regulation. It is evident that m^{6}A modification was involved in IL15RA modulation (Fig. 5D). Then, METTL3 was overexpressed (Figure S4B) to check whether the level of IL15RA mRNA is influenced. The data from Fig. 5E-F demonstrated that METTL3 upregulates IL15RA expression in both cell lines. Further MeRIP-PCR test proved that m^{6}A increases in IL15RA mRNA is mainly caused by METTL3 (Fig. 5G-H). With the probable m^{6}A sites predicted by SRAMP (Fig. 5I), the constructs with predicted sites mutated were applied in the dual luciferase assay to confirm that the site 1219 is the m^{6}A binding region (Fig. 5J). Further RNA decay assay showed that METTL3 mediated m^{6}A modification is involved in sustaining IL15RA mRNA stability (Fig. 5K). With IL15RA was manipulated (Figure S4C-D), results of wound healing and transwell migration test validated the prediction from Fig. 5L-O, that is, IL15RA is a driver for metastasis of ccRCC.

IL15RA potentiates CcRCC metastasis in vivo

As the data shown in Fig. 5, IL15RA modulated ccRCC invasion and migration in vitro. Then, it is necessary to verified it in vivo. Figure 6A showed the way OSRC-2 cells injected. It is obviously, IL15RA overexpression could enhance proliferation of ccRCC, while IL15RA knockdown repressed the growth of ccRCC in vivo (Fig. 6B-D). Notably, the metastasis of ccRCC was potentiated under IL15RA overexpression, and was inhibited in the IL15RA silencing condition ((Fig. 6E-F, $P<0.001$).

IL15RA potentiates metastasis via NF-κB/ZEB1 axis in CcRCC

The modulated pathway of IL15RA in ccRCC is the next to ascertain in this study. As indicated in Fig. 2B, NF-κB pathway may be the biological process related to IL15RA. Thus, the expression of p-p65 was measured in OSRC-2 or ACHN cell line with IL15RA overexpression or knock down as Figure S4C-D showed. Figure 7A-C demonstrated that the protein level of p-p65 increased when IL15RA protein expression was upregulated, the trend was reversed with NF-κB inhibitor JSH-23. In the contrary, the protein level of p-p65 was decreased when IL15RA protein expression was downregulated, NF-κB activator-1 (NF-κB activator) can rescue p-p65 protein expression Fig. 7D-F).

The EMT associated genes were tested to confirm the target genes that modulated by NF-κB pathway in IL15RA overexpression in both cell lines. The results showed that ZEB1 is upregulated with IL15RA overexpression in vitro (Fig. 7G). Then how p-p65 control ZEB1 expression? A dual luciferase assay with plasmids that carried different binding sites was performed to identify the exact binding site of p-p65 for ZEB1 promoter region (Fig. 7H). JSH-23 could block the binding of p-p65 to the promoter region of ZEB1. Conversely, NF-κB activator-1 could enhance the binding of p-p65 to the promoter region of ZEB1(Fig. 7I). The subsequent assay confirmed that p-p65 binds to the locus −569 to −560 of ZEB1 promoter to affect ZEB1 transcription (Fig. 7J).

Taken together, it is concluded that STAT1 and METTL3-mediated IL15RA expression modulates metastasis via NF-κB/ZEB1 Axis in ccRCC (Fig. 7K).

High IL15RA expression confers improved chemotherapy efficacy in CcRCC

In clinical treatment, chemotherapy is still a necessary strategy in tumor therapy. So, common chemotherapy drugs from previous study were collected to explore the relationship between drug sensitivity and IL15RA expression[34]. The drug sensitivity of sunitinib, pyrimethamine, cisplatin, bosutinib, imatinib, cytarabine, paclitaxel gefitinib, lenalidomide were considerably more improved in the high-IL15RA group than the low-IL15RA group (Fig. 8), and the drug sensitivity of rapamycin and gefitinib showed no difference between the two groups (data not shown). In short, these results indicate that patients with high expression of IL15RA may receive better drug treatment efficacy.

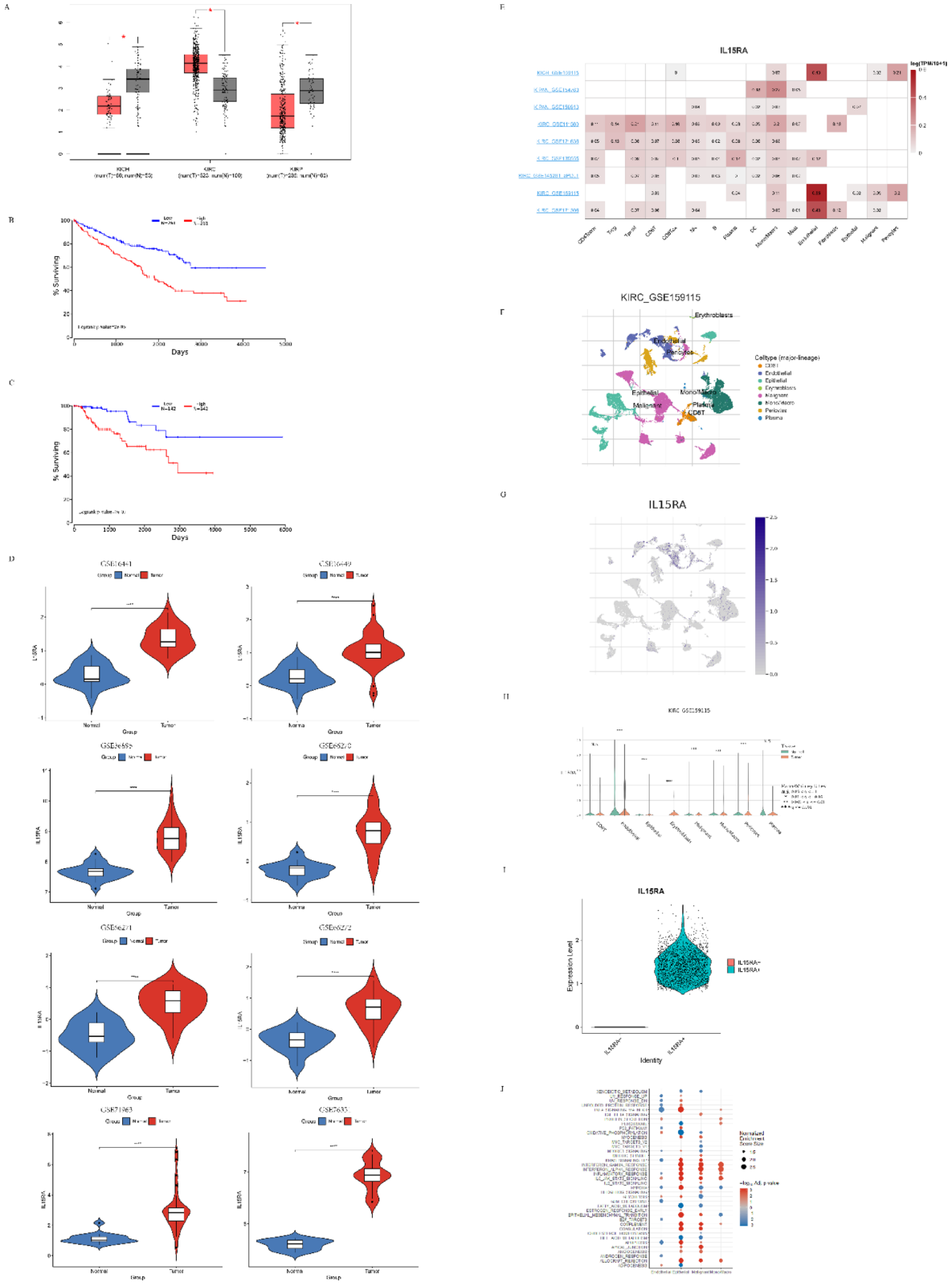

Discussion

With integrated bioinformatics analysis approaches, it is concluded that IL15RA is a potential biomarker for disease diagnosis, prognostic inference, and immunotherapy. IL15RA expression is influenced by various factors, and when considering treatments targeting IL15RA, it is important to weigh the potential risks associated with its functional role. Our research provides new insights for the diagnosis and treatment of ccRCC and some directions for the study of IL15RA in other diseases.

Compared to IL15, IL15RA received less attention. There have been multiple reports on research of IL15 and IL15RA, especially IL15 in tumor therapy[35,36]. Interestingly, our functional analysis shows that

◀**Fig. 4**. Expression, prognosis and single-cell analysis of IL15RA in ccRCC. (A). IL15RA expression between normal and tumor in TCGA and GTEx datasets from GEPIA2. (B). OS analysis of IL15RA in KIRC in UALCAN. (C). OS analysis of IL15RA in KIRP in UALCAN. (D). Expression analysis of IL15RA between normal and tumor from GSE16441, GSE16449, GSE36895, GSE66270, GSE66271, GSE66272, GSE71963 and GSE76351. (E). Single-cell analysis of IL15RA.Single-cell analysis of IL15RA in kidney cancer. (F-G). Single-cell analysis of IL15RA in ccRCC datasets GSE159115. (H). Expression analysis of IL15RA in GSE159115 between normal and tumor tissues. (I). Expression analysis of IL15RA in GSE159115 between IL15RA- and IL15RA + cells. (J). GSEA analysis of IL15RA- and IL15RA + cells in GSE159115 based on different cell types. $^{*}P < 0.05$, $^{**}P < 0.01$., $^{***}P < 0.001$.

IL15RA is involved in immune-related pathways in cancer. Our integrated analysis at the pan-cancer level demonstrated that IL15RA serves as a potential immunotherapy biomarker in various tumors, especially in cancer.

After comprehensive analysis, we finally selected ccRCC and preformed further investigation. Studies reveal that human renal cancer cells express a novel membrane-bound interleukin-15 that induces, in response to the soluble interleukin-15 receptor alpha chain, epithelial to mesenchymal transition[37]. Same authors also found that human renal normal, tumoral, and cancer stem cells express membrane-bound interleukin-15 isoforms displaying different functions[38]. These studies have documented functional investigations of exogenous soluble IL15RA. Despite the initial focus is on IL15RA, the subsequent research emphasis was ultimately shifted to the IL15/IL15RA axis. In addition, we found that previous study has constructed a prognostic model with four genes including IL15RA which can also partially confirm the our findings[39].

Unlike the perfect prognosis analysis showed in the research by Yu et al.[40], we focused on the possible immunotherapeutic value and genetic regulation of IL15RA across all cancers. Instead of professional analysis with complicated calculation, we provided our data with accessible online platforms to enlighten readers to carry out the initial explorations with ease.

Optimized dynamic network Biomarker (ODB) algorithm is widely used in biomarker screening for immunotherapy[41]. The method has been successfully employed to detect biomarkers of kidney cancer in recent years, but no such data on IL15RA has been published. We believe that future reports with ODB algorithm on IL15RA would further support our findings.

As to immunotherapy response, we showed immunotherapy response of IL15RA in murine model, cell line and publicly shared database. Nevertheless, the relationship between certain signature genes and immunotherapy response in kidney cancer is still unclear. For example, the unidentified association of DNA damage repair (DDR) associated signature genes[42] or mitochondrial pathway signature genes[43] between immunotherapy response, which would potentially restrain us from unveiling IL15RA's immunoregulatory role within the tumor microenvironment and its relationship to metastatic pathways.

Immunotherapy in ccRCC has been widely accepted to date, but combination therapy is still recommended in advanced stage ccRCC treatment. Emerging treatments such as novel target inhibitor design developed drugs[44] and computer designed chemotherapeutic drug derivatives[45] offer alternative strategies for advanced stage ccRCC patients in future.

Several potential limitations should be considered for our findings, although we have performed an integrated analysis of IL15RA. Firstly, our study mainly focused on public data due to lack of clinical samples, more powerful studies are needed to confirm the current findings. Secondly, our study mainly focused on mRNA level expression analysis with multiple datasets, a certain scale of protein level expression studies is worth doing and it would also make more sense to do some cell experiments. Thirdly, more crucial information still needs to be discovered due to shortcomings of our bioinformatic analysis. The value of IL15RA in tumors should be further validated through more in vitro and in vivo experiments.

In conclusion, our findings provided that IL15RA is a plausible biomarker for cancer treatment and it would especially benefit mechanism elucidation, prevention and therapy of ccRCC.

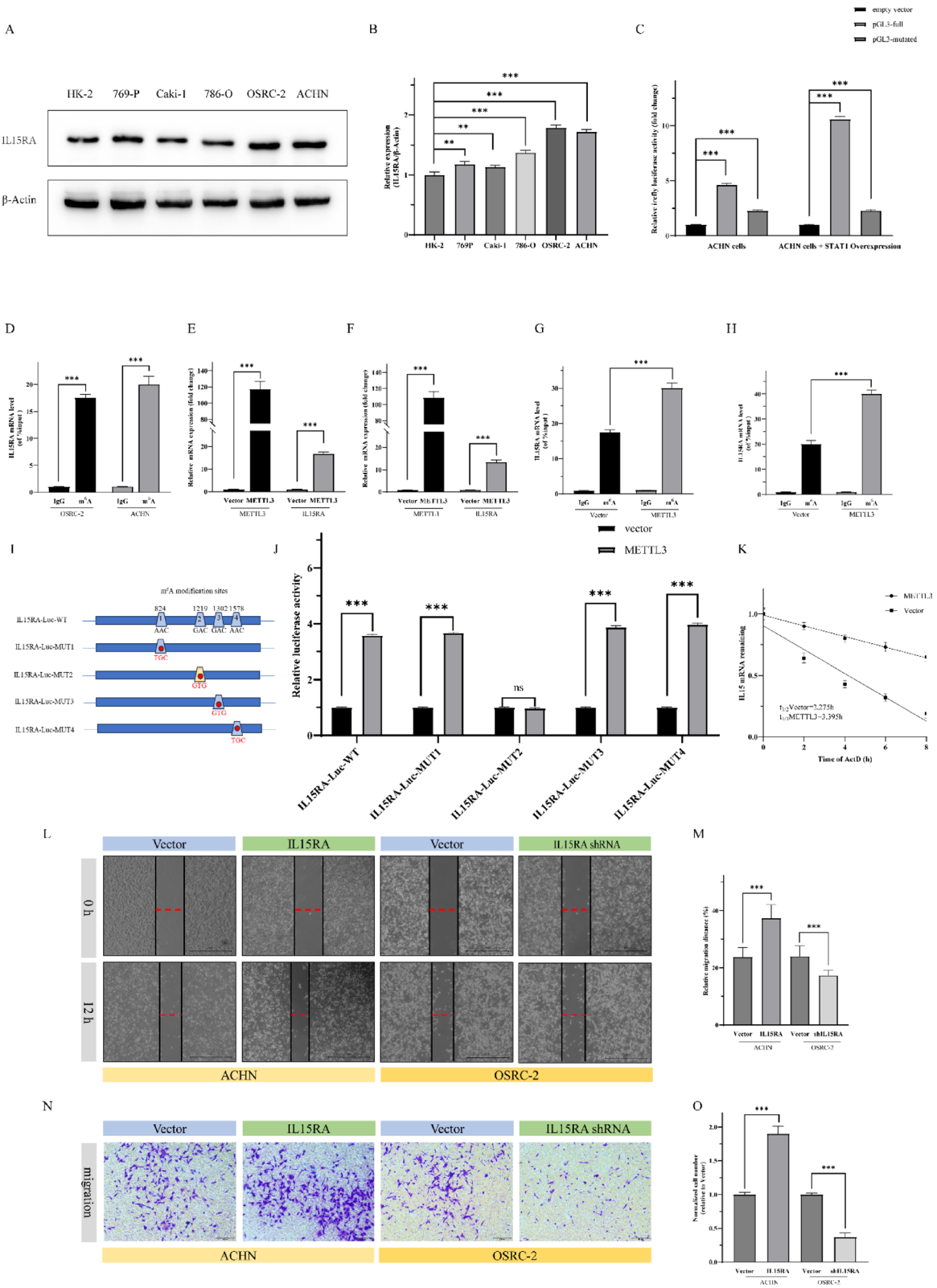
A
HK-2
769-P
Caki-1
786-O
OSRC-2
ACHN
IL15RA
β-Actin
B
Relative expression (IL15RA/β-Actin)
C
empty vector
pGL3-full
pGL3-mutated
Relative firefly luciferase activity (fold change)
ACHN cells
ACHN cells + STAT1 Overexpression
D
IL15RA mRNA level (of %input)
IgG
m6A
OSRC-2
ACHN
E
Relative mRNA expression (fold change)
Vector
METTL3
F
G
vector
METTL3
H
I
m6A modification sites
824
1219
1302
1578
IL15RA-Luc-WT
IL15RA-Luc-MUT1
IL15RA-Luc-MUT2
IL15RA-Luc-MUT3
IL15RA-Luc-MUT4
J
Relative luciferase activity
ns
K
IL15 mRNA remaining
Time of ActD (h)
L
Vector
IL15RA
IL15RA shRNA
0 h
12 h
ACHN
OSRC-2
M
Relative migration distance (%)
N
migration
O
Normalized cell number (relative to Vector)

◂**Fig. 5**. The role of IL15RA in genetic and epigenetic regulation, cell migration of ccRCC. (A-B). Western blotting results of IL15RA in cell lines and quantification statistical bar graph. (C). Dual luciferase assay indicated that STAT1 modulates IL15RA transcription activity in ACHN cell line. (D). Overexpression of METTL3 upregulates IL15RA expression in OSRC-2 and ACHN cell lines. (E-F). qRT-PCR results of IL15RA mRNA in OSRC-2 and ACHN cell lines with METTL3 overexpression. (G-H). MeRIP-PCR results of IL15RA mRNA in OSRC-2 and ACHN cell lines with METTL3 overexpression. (I). SRAMP online tool predicted m^{6}A binding sites. (J). Dual luciferase assay indicated that site 1219 is the m6A binding site of IL15RA mRNA that modulates IL15RA transcription activity in HEK 293 T cell line. (K). RNA decay assay results of IL15RA mRNA in ACHN cell line with METTL3 overexpression. (L-M). Wound closure test results of IL15RA overexpression and silencing in cell lines and quantification statistical bar graph. (N-O). Transwell migration assay results of IL15RA overexpression and silencing in cell lines and quantification statistical bar graph. $^*P<0.05$; $^{**}P<0.01$; $^{***}P<0.001$.

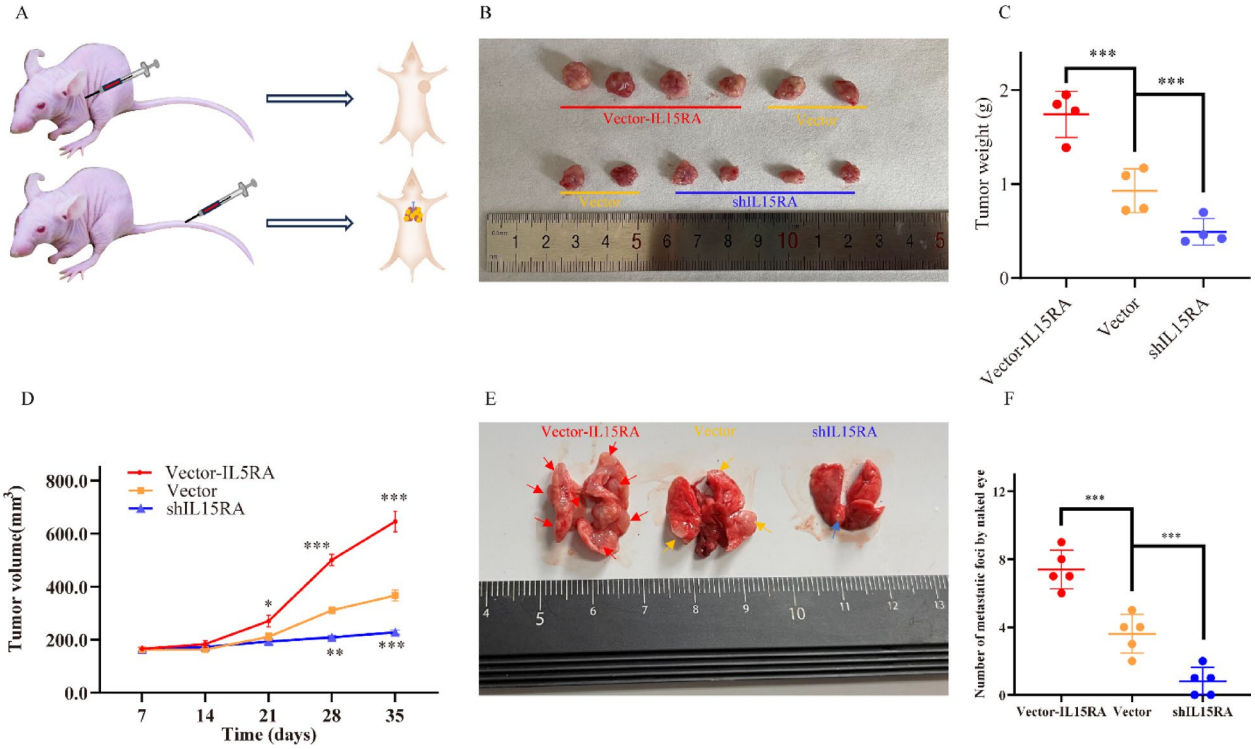

Fig. 6. IL15RA potentiates ccRCC Metastasis in vivo. (A). OSRC-2 cells with IL15RA overexpression or IL15RA knockdown. (B). Tumor grafts got in vivo. (C). The weight comparison of tumor grafts in B. (D). The tumor volumes measured each week for tumor proliferation. (E). Representative samples for metastasis comparison. (F). Comparison of metastatic foci by naked eye in different groups. $^*P<0.05$; $^{**}P<0.01$; $^{***}P<0.001$.

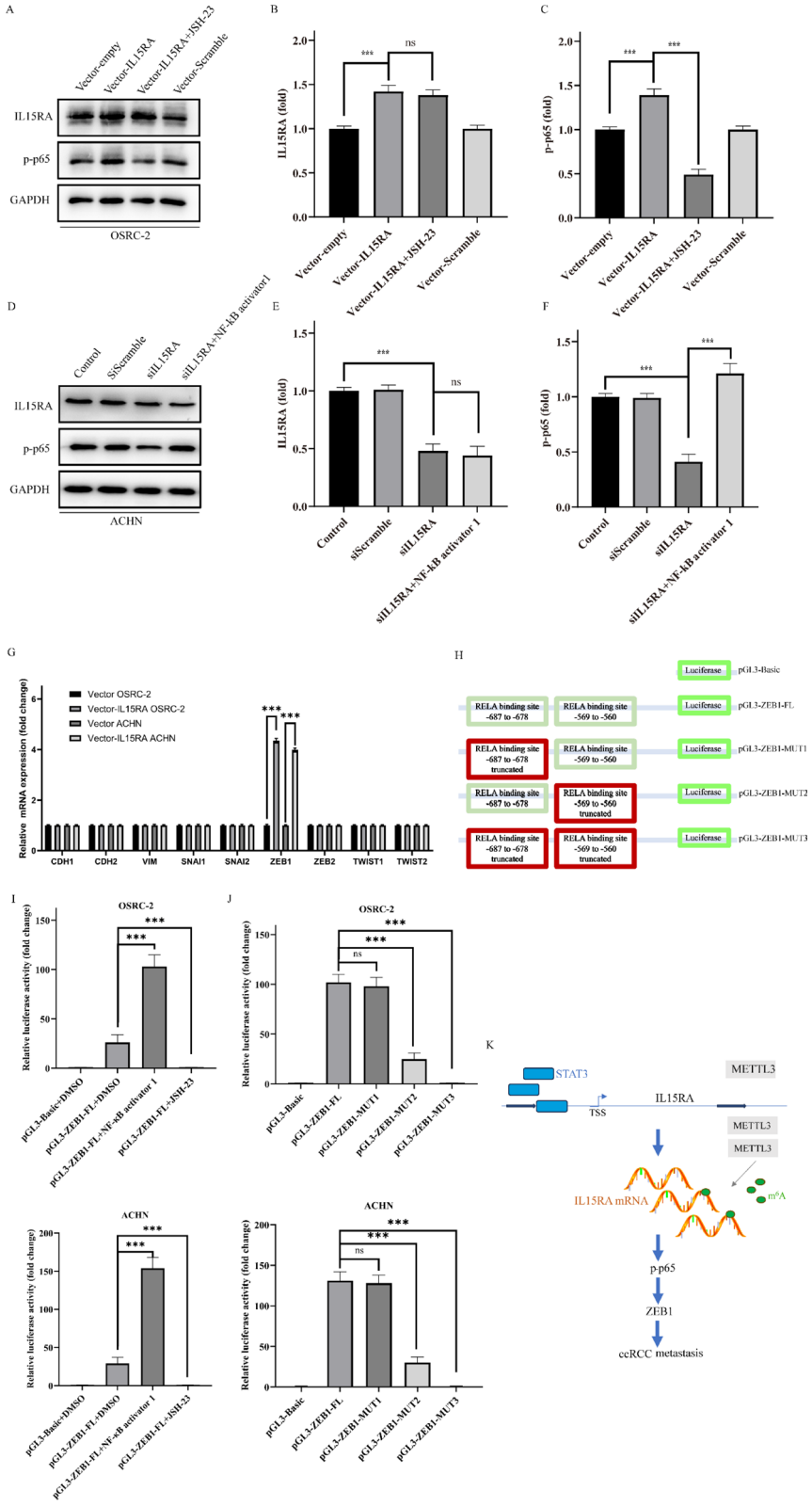
A
Vector-empty
Vector-IL15RA
Vector-IL15RA+JSH-23
Vector-Scramble
IL15RA
p-p65
GAPDH
OSRC-2
B
IL15RA (fold)
ns
***
C
p-p65 (fold)
D
Control
SiScramble
siIL15RA
siIL15RA+NF-kB activator1
ACHN
E
F
G
Vector OSRC-2
Vector-IL15RA OSRC-2
Vector ACHN
Vector-IL15RA ACHN
Relative mRNA expression (fold change)
CDH1
CDH2
VIM
SNAI1
SNAI2
ZEB1
ZEB2
TWIST1
TWIST2
H
Luciferase
pGL3-Basic
RELA binding site -687 to -678
RELA binding site -569 to -560
pGL3-ZEB1-FL
RELA binding site -687 to -678 truncated
pGL3-ZEB1-MUT1
pGL3-ZEB1-MUT2
pGL3-ZEB1-MUT3
I
OSRC-2
Relative luciferase activity (fold change)
pGL3-Basic+DMSO
pGL3-ZEB1-FL+DMSO
pGL3-ZEB1-FL+NF-kB activator 1
pGL3-ZEB1-FL+JSH-23
J
pGL3-Basic
pGL3-ZEB1-FL
pGL3-ZEB1-MUT1
pGL3-ZEB1-MUT2
pGL3-ZEB1-MUT3
ACHN
K
STAT3
IL15RA
TSS
METTL3
IL15RA mRNA
m6A
p-p65
ZEB1
ccRCC metastasis

◀**Fig. 7**. IL15RA potentiates metastasis via NF-κB/ZEB1 Axis in ccRCC. (A). Western blotting result of p-p65 protein expression in IL15RA overexpression with or without JSH-23. (B). Quantification analysis of IL15RA protein expression in different groups of A. (C). Quantification analysis of p-p65 protein expression in different groups of A. (D). Western blotting result of p-p65 protein expression in IL15RA knockdown with or without NF-κB activator-1. (E). Quantification analysis of IL15RA protein expression in different groups of D. (F). Quantification analysis of p-p65 protein expression in different groups of D. (G). Expression of EMT associated genes in IL15RA overexpression condition in OSRC-2 and ACHN cell lines. (H). Vectors including possible binding sites of p-p65 for ZEB1 promoter region were constructed for dual luciferase assays. (I). Results of luciferase assay performed with ZEB1 full promoter region vector and JSH-23 or NF-κB activator-1 in both cell lines. (J). Results of luciferase assay performed with different ZEB1 promoter region vector and IL15RA overexpression in both cell lines. (K). The schematic map for IL15RA regulation in ccRCC. $^{*}P<0.05$; $^{**}P<0.01$; $^{***}P<0.001$.

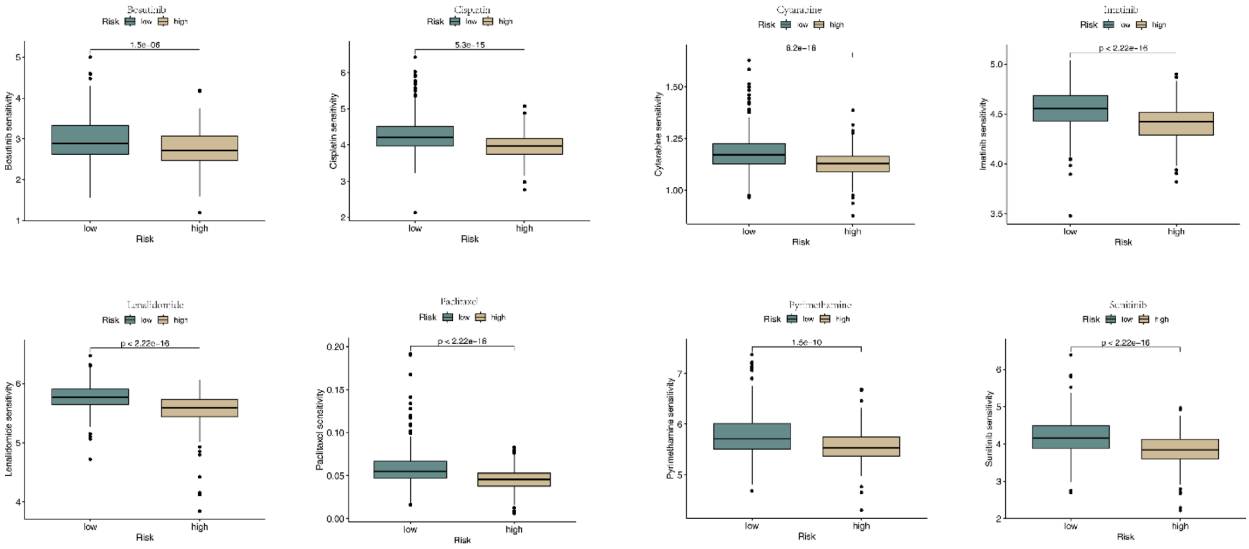

Fig. 8. Drug sensitivity analysis of the low-IL15RAand high-IL15RA groups in TCGA-KIRC. The drug sensitivity showed significant differences between the low-IL15RA and high-IL15RA groups for sunitinib, pyrimethamine, cisplatin, bosutinib, imatinib, cytarabine, paclitaxel gefitinib, lenalidomide.

Data availability

All bioinformatic web tools or public datasets used in the current study are described in detail in the manuscript, the data that support the findings of this study are available from the corresponding author upon reasonable request.

Received: 25 April 2025; Accepted: 24 September 2025
Published online: 30 October 2025

References

1. Wu, Z., Xia, F. & Lin, R. Global burden of cancer and associated risk factors in 204 countries and territories, 1980–2021: a systematic analysis for the GBD 2021. *J. Hematol. Oncol.* **17**, 119. https://doi.org/10.1186/s13045-024-01640-8 (2024).
2. Sung, H. et al. Global cancer statistics 2020: GLOBOCAN estimates of incidence and mortality worldwide for 36 cancers in 185 countries. *Ca-Cancer J. Clin.* **71**, 209–249. https://doi.org/10.3322/caac.21660 (2021).
3. Sharma, P., Hu-Lieskovan, S., Wargo, J. A., Ribas, A. & Primary Adaptive, and acquired resistance to cancer immunotherapy. *Cell* **168**, 707–723. https://doi.org/10.1016/j.cell.2017.01.017 (2017).
4. Luo, Z. et al. Exercise-induced IL-15 acted as a positive prognostic implication and tumor-suppressed role in pan-cancer. *Front. Pharmacol.* **13**, 1053137. https://doi.org/10.3389/fphar.2022.1053137 (2022).
5. Chirifu, M. et al. Crystal structure of the IL-15–IL-15Rα complex, a cytokine-receptor unit presented in trans. *Nat. Immunol.* **8**, 1001–1007. https://doi.org/10.1038/ni1492 (2007).
6. Bessard, A., Solé, V., Bouchaud, G., Quéméner, A. & Jacques, Y. High antitumor activity of RLI, an interleukin-15 (IL-15)–IL-15 receptor α fusion protein, in metastatic melanoma and colorectal cancer. *Mol. Cancer Ther.* **8**, 2736–2745. https://doi.org/10.1158/1535-7163.Mct-09-0275 (2009).
7. Guo, S., Smeltz, R. B., Nanajian, A. & Heller, R. IL-15/IL-15Rα heterodimeric complex as cancer immunotherapy in murine breast cancer models. *Front. Immunol.* **11**, 614667. https://doi.org/10.3389/fimmu.2020.614667 (2021).
8. Kurz, E. et al. Exercise-induced engagement of the IL-15/IL-15Rα axis promotes anti-tumor immunity in pancreatic cancer. *Cancer Cell.* **40**, 720–737e725. https://doi.org/10.1016/j.ccell.2022.05.006 (2022).
9. Zhang, W. et al. Crosstalk between IL-15Rα + tumor-associated macrophages and breast cancer cells reduces CD8 + T cell recruitment. *Cancer Commun.* **42**, 536–557. https://doi.org/10.1002/cac2.12311 (2022).

10. Wu, D. et al. IL15RA-STAT3-GPX4/ACSL3 signaling leads to ferroptosis resistance in pancreatic cancer. *Acta Biochim. Biophys. Sin.* **57**, 389–402. https://doi.org/10.3724/abbs.2024153 (2024).
11. Wang, J. T. F. T. F. An R-Based integrative tool for decoding human transcription Factor–Target interactions. *Biomolecules* **14**, 749. https://doi.org/10.3390/biom14070749 (2024).
12. Liu, X. S. et al. TIMER2.0 for analysis of tumor-infiltrating immune cells. *Nucleic Acids Res.* **48**, W509–W514. https://doi.org/10.1093/nar/gkaa407 (2020).
13. Liao, C. & Wang, X. TCGAplot: an R package for integrative pan-cancer analysis and visualization of TCGA multi-omics data. *BMC Bioinform.* **24**, 483. https://doi.org/10.1186/s12859-023-05615-3 (2023).
14. Wang, J. et al. A common housekeeping gene with an oncogenic role in pan-cancer. *Comput. Struct. Biotechnol. J. 21*. **GAPDH**, 4056–4069. https://doi.org/10.1016/j.csbj.2023.07.034 (2023).
15. Tang, Z., Kang, B., Li, C., Chen, T. & Zhang, Z. GEPIA2: an enhanced web server for large-scale expression profiling and interactive analysis. *Nucleic Acids Res.* **47**, W556–W560. https://doi.org/10.1093/nar/gkz430 (2019).
16. Chandrashekar, D. S. et al. UALCAN: A portal for facilitating tumor subgroup gene expression and survival analyses. *Neoplasia* **19**, 649–658. https://doi.org/10.1016/j.neo.2017.05.002 (2017).
17. Zheng, X. et al. DMRdb: a disease-centric Mendelian randomization database for systematically assessing causal relationships of diseases with genes, proteins, CpG sites, metabolites and other diseases. *Nucleic Acids Res.* **53**, D1363–D1371. https://doi.org/10.1093/nar/gkae853 (2025).
18. Chen, D. et al. Sangerbox 2: Enhanced functionalities and update for a comprehensive clinical bioinformatics data analysis platform. *iMeta* **3**, e238. https://doi.org/10.1002/imt2.238 (2024).
19. Yu, G., Wang, L. G., Han, Y. & He, Q. Y. ClusterProfiler: an R package for comparing biological themes among gene clusters. *OMICS* **16**, 284–287. https://doi.org/10.1089/omi.2011.0118 (2012).
20. Subramanian, A. et al. Gene set enrichment analysis: A knowledge-based approach for interpreting genome-wide expression profiles. *P Natl. Acad. Sci. USA*. **102**, 15545–15550. https://doi.org/10.1073/pnas.0506580102 (2005).
21. Wu, H., Geng, Q., Shi, W. & Qiu, C. Comprehensive pan-cancer analysis reveals CCDC58 as a carcinogenic factor related to immune infiltration. *Apoptosis* **29**, 536–555. https://doi.org/10.1007/s10495-023-01919-0 (2024).
22. Charoentong, P. et al. Pan-cancer Immunogenomic analyses reveal Genotype-Immunophenotype relationships and predictors of response to checkpoint Blockade. *Cell. Rep.* **18**, 248–262. https://doi.org/10.1016/j.celrep.2016.12.019 (2017).
23. Jiang, P. et al. Signatures of T cell dysfunction and exclusion predict cancer immunotherapy response. *Nat. Med.* **24**, 1550–1558. https://doi.org/10.1038/s41591-018-0136-1 (2018).
24. Fu, J. et al. Large-scale public data reuse to model immunotherapy response and resistance. *Genome Med.* **12**, 21. https://doi.org/10.1186/s13073-020-0721-z (2020).
25. Zeng, Z. et al. TISMO: syngeneic mouse tumor database to model tumor immunity and immunotherapy response. *Nucleic Acids Res.* **50**, D1391–D1397. https://doi.org/10.1093/nar/gkab804 (2022).
26. Nagy, Á., Győrffy, B. & muTarget A platform linking gene expression changes and mutation status in solid tumors. *Int. J. Cancer*. **148**, 502–511. https://doi.org/10.1002/ijc.33283 (2020).
27. Sun, D. et al. TISCH: a comprehensive web resource enabling interactive single-cell transcriptome visualization of tumor microenvironment. *Nucleic Acids Res.* **49**, D1420–D1430. https://doi.org/10.1093/nar/gkaa1020 (2021).
28. Han, Y. et al. TISCH2: expanded datasets and new tools for single-cell transcriptome analyses of the tumor microenvironment. *Nucleic Acids Res.* **51**, D1425–D1431. https://doi.org/10.1093/nar/gkac959 (2023).
29. Wang, H., Wang, J., Li, D., Zhu, Z. & Pei, D. A functional polymorphism within the distal promoter of RUNX3 confers risk of colorectal cancer. *Int. J. Biol. Markers*. **37**, 40–46. https://doi.org/10.1177/17246008211073342 (2022).
30. Fan, R. et al. A combined deep learning framework for mammalian m6A site prediction. *Cell. Genom.* **4**, 100697. https://doi.org/10.1016/j.xgen.2024.100697 (2024).
31. Dreos, R., Ambrosini, G., Perier, R. C. & Bucher, P. The eukaryotic promoter database: expansion of EPDnew and new promoter analysis tools. *Nucleic Acids Res.* **43**, D92–96. https://doi.org/10.1093/nar/gku1111 (2015).
32. Yang, W. et al. Genomics of drug sensitivity in cancer (GDSC): a resource for therapeutic biomarker discovery in cancer cells. *Nucleic Acids Res.* **41**, D955–D961. https://doi.org/10.1093/nar/gks1111 (2012).
33. Maeser, D., Gruener, R. F. & Huang, R. S. OncoPredict: an R package for predicting in vivo or cancer patient drug response and biomarkers from cell line screening data. *Brief. Bioinform.* **22**, bbab260. https://doi.org/10.1093/bib/bbab260 (2021).
34. Dong, P. et al. A model based on Immunogenic cell death-related genes predicts prognosis and response to immunotherapy in kidney renal clear cell carcinoma. *Translational Cancer Res.* **13**, 249–267. https://doi.org/10.21037/tcr-23-214 (2024).
35. Wu, Y. et al. Thermal-responsive activation of engineered bacteria to trigger antitumor immunity post microwave ablation therapy. *Nat. Commun.* **15**, 10503. https://doi.org/10.1038/s41467-024-54883-x (2024).
36. Zhou, Y. et al. The application of Interleukin-2 family cytokines in tumor immunotherapy research. *Front. Immunol.* **14**, 10903. https://doi.org/10.3389/fimmu.2023.1090311 (2023).
37. Tejman-Yarden, N. et al. Renal cells express a functional interleukin-15 receptor. *Nephrol. Dial Transpl.* **20**, 516–523. https://doi.org/10.1093/ndt/gfh616 (2005).
38. Khawam, K. et al. Human renal cancer cells express a novel membrane-bound interleukin-15 that induces, in response to the soluble interleukin-15 receptor alpha chain, epithelial-to-mesenchymal transition. *Cancer Res.* **69**, 1561–1569. https://doi.org/10.1158/0008-5472.CAN-08-3198 (2009).
39. Azzi, S. et al. Human renal Normal, Tumoral, and cancer stem cells express Membrane-Bound Interleukin-15 isoforms displaying different functions. *Neoplasia* **17**, 509–517. https://doi.org/10.1016/j.neo.2015.06.002 (2015).
40. Yu, Q. X. et al. An inflammation-related signature could predict the prognosis of patients with kidney renal clear cell carcinoma. *Front. Genet.* **13**, 866696. https://doi.org/10.3389/fgene.2022.866696 (2022).
41. Zhang, H. et al. Optimized dynamic network biomarker Deciphers a High-Resolution heterogeneity within thyroid cancer molecular subtypes. *Med. Res.* **1**, 10–31. https://doi.org/10.1002/mdr2.70004 (2025). https://doi.org:
42. Zhang, P. et al. Clinical prognostication and immunotherapy response prediction in esophageal squamous cell carcinoma using the DNA damage repair-associated signature. *Environ. Toxicol.* **39**, 2803–2816. https://doi.org/10.1002/tox.24155 (2024).
43. Zhang, P. et al. Mitochondrial pathway signature (MitoPS) predicts immunotherapy response and reveals NDUFB10 as a key immune regulator in lung adenocarcinoma. *J. Immunother Cancer*. **13**, e012069. https://doi.org/10.1136/jitc-2025-012069 (2025).
44. Ma, Y. C. et al. Identification of novel inhibitor of protein tyrosine phosphatases delta: structure-based pharmacophore modeling, virtual screening, flexible docking, molecular dynamics simulation, and post-molecular dynamics analysis. *J. Biomol. Struct. Dyn.* **38**, 4432–4448. https://doi.org/10.1080/07391102.2019.1682050 (2020).
45. Yang, B., Li, X., He, L. & Zhu, Y. Computer-aided design of Temozolomide derivatives based on alkylglycerone phosphate synthase structure with isothiocyanate and their pharmacokinetic/toxicity prediction and anti-tumor activity in vitro. *Biomed. Rep.* **8**, 235–240. https://doi.org/10.3892/br.2018.1051 (2018).

Acknowledgements

We thank the technicians that help us to obtain the results of the current study.

Author contributions

Conceptualization, J.W., X.Z. and Z.Z.; methodology, J.W. C.W. and X.Z.; software, J.W., C.W. and Y.G.; validation, X.Z., X.G. and Z.Z.; formal analysis, J.W. and X.Z.; investigation, J.W. and X.Z.; resources, R.L.; data curation, X.L., Z.S. and Z.Z.; writing—original draft preparation, J.W. and Z.Z.; writing-review and editing, R.L. and Z.Z; visualization, X.L. and J.W.; supervision, Z.Z.; project administration, Z.Z.; funding acquisition, X.Z., H.W. and R.L. All authors have read and agreed to the published version of the manuscript.

Funding

This research was funded by Xuzhou Medical University Undergraduate Training Program for Innovation and Entrepreneurship (No. 202410313040Y to X.Z.), the Key Research and Development Program of Xuzhou City (No. KC22193 to R.L. and No. KC22125 to H.W.).

Declarations

Competing interests

The authors declare no competing interests.

Ethical approval

All animal assays were performed in accordance with protocols approved by the Institutional Animal Care and Use Committee at Xuzhou Medical University (No.202207S064).

Additional information

Supplementary Information The online version contains supplementary material available at https://doi.org/10.1038/s41598-025-21947-x.

Correspondence and requests for materials should be addressed to R.L. or Z.Z.

Reprints and permissions information is available at www.nature.com/reprints.

Publisher's note Springer Nature remains neutral with regard to jurisdictional claims in published maps and institutional affiliations.